High Resolution Prediction of Gas Injection Process Performance for Heterogeneous Reservoirs

Quarterly Report
January 1, 2003 to March 31, 2003

Contract No. DE-FC26-00BC15319

Principal Investigator: Franklin M. Orr, Jr.
Department of Petroleum Engineering
Stanford University

Disclaimer

Abstract

This report outlines progress in the second quarter of the third year of the DOE project “High Resolution Prediction of Gas Injection Process Performance for Heterogeneous Reservoirs”.

This report presents results of an investigation of the effects of variation in interfacial tension (IFT) on three-phase relative permeability. We report experimental results that demonstrate the effect of low IFT between two of three phases on the three-phase relative permeabilities. In order to create three-phase systems, in which IFT can be controlled systematically, we employed analog liquids composing of hexadecane, n-butanol, isopropanol, and water. Phase composition, phase density and viscosity, and IFT of three-phase system were measured and are reported here. We present three-phase relative permeabilities determined from recovery and pressure drop data using the Johnson-Bossler-Naumann (JBN) method. The phase saturations were obtained from recovery data by the Welge method.

The experimental results indicate that the wetting phase relative permeability was not affected by IFT variation whereas the other two-phase relative permeabilities were clearly affected. As IFT decreases the “oil” and “gas” phases become more mobile at the same phase saturations.

Contents

1. Executive Summary

Variations in gas and oil relative permeabilities as a function of interfacial tension (IFT) are of particular importance in the area of compositional processes like high-pressure gas injection, where oil and gas compositions can vary significantly both spatially and temporally. With presence of water (in a pre-waterflooded reservoir or WAG processes), gas injection processes routinely include three-phase flow. Hence, the effect of IFT variations on three-phase relative permeabilities must be delineated if the performance of gas injection process is to be predicted accurately. In this study we report an experimental investigation of the effect of IFT variations on the three-phase relative permeabilities.

In order to create three-phase systems in which IFT can be controlled systematically, we employed analog liquids composing of hexadecane (C_{16}), n-butanol (NBA), isopropanol (IPA), and water (H_2O). This approach offers some flexibility in the design of displacement experiments to investigate effects of IFT in three-phase flow. For example, injection of pre-equilibrated three-phase fluids should allow control of IFT between pairs of phases with low IFT between one pair. Phase compositions, phase densities and viscosities, and IFT of three-phase systems were measured and are reported here. Displacements were performed in a pack of Teflon beads. In this system, **the C_{16}-rich phase** represents the wetting phase (corresponding to **water** in a water-wet reservoir system), **the NBA-rich phase** represents the intermediate wetting phase (corresponding to **the oil phase** in a water-wet reservoir system), and **the H_2O-rich phase** represents the most non-wetting phase (corresponding to **the gas phase** in a water-wet reservoir system).

Three dynamic displacement experiments with IFTs of 0.028, 0.308, and 2.297 mN/m were performed for displacements of NBA-rich phase (“oil”) by H_2O-rich phase (“gas”) in the presence of C_{16}-rich phase (“water”). The relevant three-phase relative permeabilities were obtained from the recovery and pressure drop data by applying the Johnson-Bossler-Naumann (JBN) method. The experimental results indicate that the water phase relative permeability was not affected by the IFT variation whereas the relative permeabilities of the phases were clearly affected. As IFT decreases the “oil” and “gas” phases become more mobile at the same phase saturations.

2. Introduction

Variation of interfacial tension (IFT) with temperature and pressure can have significant impact on displacement performance in miscible gas injection processes (Schechter *et al.*, 1994). Because gas injection processes routinely include three-phase flow (either because the reservoir has been previously waterflooded or because water is injected alternately with gas in order to improve overall reservoir sweep efficiency), the effect of IFT variations on three-phase relative permeabilities must be delineated if the performance of gas injection process is to be predicted accurately. The development of multicontact miscibility in a gas injection process will create zones of low IFT between gas and oil phases in the presence of water.

Although there have been a few attempts to analyze the effect of low IFT on two-phase relative permeability (Table 1), there are no experimental data published so far analyzing the effect of low IFT on three-phase relative permeabilities. Because the IFT between oil and gas phases is the objective parameter for most of enhanced oil recovery techniques, almost all authors naturally focussed on the effect of IFT on oil and gas phase relative permeabilities. Experimental results show that residual oil saturation and relative permeability are strongly affected by IFT, especially when the IFT is lower than about 0.01 mN/m (corresponding to a capillary number of 10^{-2}-10^{-3}). A linear relationship between oil relative permeability and IFTs greater than the threshold value of 0.04 mN/m was found at the same gas saturation (McDougall *et al.*, 1997). Mulyadi and Amin (2001) have recently published some experimental data showing that the IFTs for each binary mixture of brine, oil and gas phases vary as pressure increases (Fig. 1). As shown from the figure, the IFT of gas/oil pair tends to go down to zero, whereas the other two IFTs of gas/brine and oil/brine pairs approach to each other until they reach at a constant value. Such variations in the IFT are supposed to appear during gas injection processes with the presence of water.

Because they allow control of IFT in experiments performed at atmospheric pressure, oil/water/alcohol systems are useful for investigations of the effects of IFT variations. Here we consider a system containing hexadecane (C_{16}), n-butyl alcohol (NBA), and H_2O, which forms three liquid phases in equilibrium. The use of analog liquid phases offers many advantages in the laboratory determination of relative permeabilities: relatively low IFT reduces capillary end effects during displacements, IFT can be varied by changing the composition, and it is possible to create two phases that have low IFT in the presence of a third phase, just as gas/oil tensions can be low while oil/water and gas/water IFTs are not. A few researchers have already presented some applications for two-phase systems, isooctane (IC_8)/isopropyl alcohol (IPA)/brine (Morrow *et al.*, 1988, Schechter *et al.*, 1994] and for three-phase systems, decane/benzyl alcohol/water [Grader and O'Meara, 1988]. IC_8 and brine forming two-phases were diluted by IPA until the IFT becomes zero. This is, of course, a good analogy to the miscible gas injection, in which the interfacial forces between the oil and gas phases become weaker, and eventually disappear.

The selection of reasonable liquid pairs with different IFT schemes for three-phase relative permeability measurements requires the knowledge of the phase behavior of appropriate components. Knickerbocker *et al.* (1982) presented the phase behavior of different

hydrocarbon-alcohol-water combinations, which yield different three-liquid-phase patterns when salt is added. They studied all possible phase patterns for combinations of 10 monohydrid alcohols, 6 even-numbered n-alkanes having from 6 to 16, water with salinity from zero to 32 cg/mL.

The C_{16}/NBA/H_2O system gives appropriate phase behavior when IPA or NaCl is added to the mixtures. Adding either IPA or NaCl changes the compositions of the three equilibrium phases that form in a way that alters IFT appreciably.

In the sections that follow we report experimental results dealing with the effect of IFT variation on the three-phase flow. First, we present results of phase composition, phase density and viscosity, and IFT measurements of three-phase C_{16}/NBA/H_2O/IPA system under ambient conditions. Secondly we describe an analogy between C_{16}/NBA/H_2O/IPA system and reservoir fluids and explain how we selected the appropriate porous medium for the analog liquids. Finally we report results of the three-phase relative permeability measurements.

3. Analog Liquids

3.1. Experimental Procedure

The chemicals used in the experiments were NBA (EM Science, 99.94%), C_{16} (Fisher Chemicals, 99.4%), IPA (Fisher Chemicals, 99.9%), and IC_8 (Fisher Chemical, 99.4%). The aqueous phase was distilled, de-ionized H_2O.

All experiments were performed at room temperature, 22±0.4 °C. All components were mixed in the 60-cc glass vials based on their weights taken with the balance with 0.001g reproducibility. After shaking the mixtures by hand the equilibrated phases separated in times that ranged from minutes to one day (depending on the IFT between pairs of phases – low IFT mixtures took longer to separate).

The equilibrated phases were sampled by syringe and transported to 1.5-cc vials for gas chromatography measurements. To prevent contamination by the phases above when sampling H_2O-rich and NBA-rich phases, a small amount of air withdrawn by syringe before sampling was pushed out in the correspondent phase to clean any contamination at the edge of the needle. Liquid phase compositions were analyzed with a Hewlett-Packard 5880A temperature programmable gas chromatograph. Satisfactory separations were obtained by using the 6'x1/8"x0.085" stainless steel column packed with 10%Carbowax 20M on 80/100 Chromosorb W-HP (Alltech Associates). The peaks for the components, C_{16}, NBA, IPA, and H_2O, were calibrated with mixtures containing known amounts of the components.

The IFTs between the phases were measured with a spinning drop tensiometer manufactured by University of Texas (Model 300), which is very reliable for low IFTs (Manning and Scriven, 1977). The tensiometer was calibrated by known IFT values of tie lines on the phase diagram of IC8/2%$CaCl_2$ H_2O/IPA system presented by Morrow *et al.* (1988).

Densities were measured gravimetrically using a 10-cc Gay-Lussac bottle. Viscosities were measured using a Cannon-Fenske viscometer.

3.2. Compositional Data

The effects of increasing IPA fraction were examined for C_{16}/NBA/H_2O mixtures that formed three phases. First of all, the base ternary phase diagram for C_{16}/NBA/H_2O system was obtained (Fig. 2). A large three-phase region surrounded by three unconnected two-phase regions was observed for the ternary system. The C_{16}-rich phase (88%)[1] contains a small amount of H_2O (approx. 0.5%). The NBA-rich phase (74%) has 17% C_{16} and 9% H_2O. Almost no C_{16} was detected in the H_2O-rich aqueous phase which contains 8% NBA. Each of the edges of the three-phase region is also a tie line for the associated two-phase region. The two-phase regions on the H_2O/NBA and H_2O/C_{16} sides of the three-phase triangle extend all the way to the binary H_2O/NBA and H_2O/C_{16} axes. In binary mixtures of C_{16} and H_2O the C_{16}-rich phase contains only C_{16} whereas a very small amount of C_{16} (0.1%) was detected in the H_2O-rich phase. The binary mixture of NBA and H_2O yields a C_{16}-rich phase consisting of 83% NBA and 17% H_2O and an H_2O-rich phase of 8% NBA and 92% H_2O. The fact that all binary mixtures of C_{16} and NBA are completely miscible at 22 °C indicates that the two-phase region connected to the tie line of three-phase region between C_{16}-rich and NBA-rich phases must lie inside the ternary triangle. As a result, there must be a critical point on the two-phase envelope associated with the C_{16}/NBA side of the three-phase region.

Based on this ternary liquid system, we added gradually IPA to obtain a quaternary phase diagram that shows a sequence of tie triangles (Fig. 3). By adding IPA to the binary mixtures of the components we also obtained ternary diagrams which represent two sides of the quaternary diagram (Figs. 4 and 5). All compositional data are summarized in Tables 2, 3, and 4.

Combining all data shown by Figs. 2, 3, 4, and 5 yields a quaternary phase diagram for the whole system, shown in Fig. 6. The arrows in Fig. 6 show the directions of change of the respective phase compositions caused by adding IPA. C is the critical end point and AC represents approximately the critical tie line. As the concentration of IPA increases, the NBA-rich and H_2O-rich phase compositions approach each other and three-phase behavior reduces to two-phase behavior at the critical tie line.

3.3. Computational Model for 3-Phase Compositional Data

In the development of compositional reservoir simulations, a reliable computational model of phase and chemical equilibria is needed. Many computational algorithms for computing phase equilibrium exist in the phase equilibria literature [Raal and Muehlbauer, 1997]. In this section, we describe our attempt to define a model of the three-phase equilibrium data.

[1] All compositions are in mass fraction unless otherwise specified.

We used SPECS Ver 4.64, a phase behavior modeling program developed by Institute of Chemical Engineering at the Technical University of Denmark, to model the phase behavior of four component (C_{16}, NBA, H_2O, IPA) three-phase system. Although it is difficult to model three-phase liquid/liquid/liquid systems, we found that, among others, the CPA (Cubic Plus Assosiation, Kontogeorgis *et al.*, 1996) using Soave-Redlich-Kwong Equation of State gives reasonable results. Fig. 7 shows the model match to the experimental data using a quadratic mixing rule with a binary interaction (k_{ij}) obtained by matching the equilibrium data. As Fig.7 shows, the model deviates from the experimental data around the critical point and at the critical tie line. Otherwise the model representation of the three-phase behavior is reasonable.

3.4. Analogy to Reservoir Fluids Based on IFT Data

As IPA concentration was increased, the IFT between H_2O-rich and NBA-rich phases decreased (Table 5 and Fig. 8). With the same increase in the IPA ratio, the IFT between C_{16}-rich and NBA-rich phases increases, whereas the IFT between C_{16}-rich and H_2O-rich phases stays almost constant. When the IFT between H_2O-rich and NBA-rich phases reaches zero, the other two IFTs become identical, which means that only two phases exist in the system. By comparison of the results with those obtained by Mulyadi and Amin (Fig. 1), for three-phase flow experiments, we can choose the H_2O-rich phase to represent the **gas** phase, the NBA-rich phase to represent the **oil** phase, and the C_{16}-rich phase to represent the **aqueous** phase.

4. Displacement Experiments

4.1. Porous Medium

Because the C_{16}-rich phase always represents the water in the reservoir system (according to the selection criterion of analog liquids presented above), we employed an oil-wet porous medium in the laboratory to simulate the fluid flow in a water-wet oil reservoir. Alternately, employing a water-wet porous medium in the flow experiments simulated displacements in an oil-wet reservoir as long as the wetting H_2O-rich phase represents the reservoir oil. Table 6 summarizes those phase correspondences for the analog displacements.

Using unconsolidated synthetic porous media for displacement experiments offers many advantages when compared to real reservoir rocks having more complicated flow networks. Sand packs and glass beads have become almost industry standard to study water-wet porous media. In fact, sand packs and glass beads can also be used to study oil-wet porous media after aging them with appropriate crude oils or asphaltenes (Buckley *et al.*, 1997). But the IPA being used in the C_{16}/NBA/H_2O mixtures as a solvent may change the wettability of the porous medium.

Morrow and McCaffery (1978) performed some experiments with compressed porous polytetrafluoroethylene (PTFE) media, to analyze wetting conditions of reservoirs. They measured a contact angle exhibited by a given fluid pair at a smooth PTFE surface to 108º for the water/air pair and 44º for the n-tetradecane/air pair, an indication that hydrocarbons are wetting and water is non-wetting to PTFE materials.

We employed PTFE powder to mimic a water-wet porous medium. The wetting situation for this porous medium was investigated in the following simple experiments. Starting from the fact that the contact angle is a measure of wettability, we employed a direct method to determine the contact angles formed by solid-liquid interfaces. The method basically includes taking images of solid-liquid-liquid interface in a PTFE capillary tubing and determination of the contact angle (Fig. 9). The method was also verified by series of capillary rise measurements. The results tabulated in Table 7 show that the C_{16}-rich phase wets the PTFE tubing more than the others, whereas the H_2O-rich phase is the most nonwetting phase. The NBA-rich phase always represents intermediate phase when all phases coexist in the tubing.

4.2. Fluids

The fluids used in the experiments are C_{16}-rich, NBA-rich, and H_2O-rich phases with three different compositions from Table 2, namely **Mix 1**, **Mix 8**, and **Mix 9**. We prepared all mixtures in a 4000-cc Erlenmeyer, waited for phase equilibrium, and checked their properties again. As illustrated in Fig. 8, the IFT between NBA-rich and H_2O-rich phases is very sensitive to the change of IPA concentration in the mixture, especially around the critical point. Because IPA is relatively volatile, special care is required in displacement experiments to avoid composition changes due to evaporation. Therefore we tried to keep the mixture from contacting air as much as possible. IFT checks before and after the experiments indicated that changes in IFT due to evaporation were small.

For the data given in Table 5, the largest viscosity contrast is about 2.5 (between the NBA-rich and H_2O-rich phases of Mix 1) and the largest density contrast is about 1.3 (between the H_2O –rich and C_{16}-rich phases of Mix 1).

4.3. Apparatus

A simplified schematic of the three-phase dynamic displacement apparatus is shown in Fig. 10. The apparatus is capable of injecting one or two phases into the porous medium. The phases are always kept in one container to avoid any non-equilibrium conditions. The pump used is Masterflex Easy-Load Pump with the capacity of 0.06-30 mL/min. The console drive of the pump allows the use of two pump heads for the injection of two different liquids simultaneously.

The core holder is made of a 3.18 cm outside diameter by 0.34 cm thick Plexiglas tube with two end plugs of the same material. Holes were drilled through both end plugs to allow fluids to enter and exit the core. The core holder was packed dry in a vertical position with PTFE

powder purchased from Aldrich. The length and diameter of the porous medium are 36.0 cm and 2.5cm, respectively. The porous medium consists of PTFE powder with 675-μm mean diameter. The porosity of the core is 59%, determined by saturating the core with C_{16}-rich phase (the so-called gravity method) and by CT scanning. The homogeneity of the PTFE porous medium was verified using a CT scanner. The injection pressure across the core is measured by an analog gauge with 0.1-psi precision. During dynamic displacement experiments we used glass vials with 0.05-mL precision to collect the effluent.

The core holder is located vertically to allow creation of a stable displacement front. Because the gas phase is represented by the denser H_2O-rich phase, this phase was injected from the bottom of the core holder to displace the less denser C_{16}-rich and NBA-rich phases.

4.4. Experimental Procedure

An expected saturation path for displacement experiments can be represented for a given mixture from the base tie triangle as shown in Fig. 11. To obtain this saturation path we used the following experimental procedure:

1. We first let the **C_{16}-rich phase ("water")** flow into the porous medium from the bottom of the core. We did not evacuate the porous medium to avoid causing any change in the composition of liquid phase containing IPA. Then we injected about five more PVs of the C_{16}-rich phase into the porous medium to make sure that the PTFE bead packs were saturated completely. We determined the porosity from the total amount of the C_{16}-rich phase stored in the pores and measured the absolute permeability of the porous medium.
2. Then we injected **the NBA-rich phase ("oil")** into the porous medium until an irreducible C_{16}-rich phase was reached. At this point we determined the effective phase permeability.
3. We simultaneously injected C_{16}-rich and NBA-rich phases with the same flow rate to set the initial condition of the porous medium before injection of the **H_2O-rich phase ("gas")**.
4. We started the dynamic displacement experiment for measuring relative permeabilities by injecting the H_2O-rich phase into the uniformly saturated porous medium.
5. We collected the effluents and measured the differential pressure across the core as a function of pore volumes injected.
6. After the experiment, we cleaned the PTFE porous medium by flooding three PVs of IPA and flashing with dry air for 24 hours before the next experiment.
7. We repeated the steps 1-6 again with another mixture having lower IFT.

4.5. Analysis Procedure

In the methods to determine saturation and relative permeabilities the following assumptions hold:

- Incompressible fluids
- One-dimensional isothermal flow in the vertical direction

- Immiscible three-phase flow, no mass transfer between phases
- Capillary effects are ignored

The graphs of the recovered pore volumes of each phase as a function of the injected pore volume are generated. The saturation of phase *i* at the outlet of the core, S_i, is given by Welge (1952) and Grader and O'Meara (1988):

$$S_i = S_i^o - L_i + Q\frac{dL_i}{dQ} \tag{1}$$

where S_i^o is the initial saturation of phase *i* before injecting the third phase, L_i is the PV recovery of phase *i*, and *Q* is the PV of the third phase injected. Fig. 12 shows graphically how Eq. 1 is applied to determine the saturations at the end of the core.

The relative permeability to phase *i*, k_{ri}, is calculated using the following equation, including gravity,

$$k_{ri} = \frac{q_t \mu_i l}{kA}\frac{f_i}{\left((\Delta p)_{X=1} - \rho_i g l\right)} \tag{2}$$

where $(\Delta p)_{X=1}$ is the differential pressure at the downstream end of the core, which is defined by Johnson *et al.* (1958) as

$$(\Delta p)_{X=1} = \Delta p - Q\frac{d(\Delta p)}{dQ} \tag{3}$$

where q_t is the total flow rate, μ_i the viscosity of phase *i*, *l* the length of the core, f_i the fractional flow of phase *i*, *k* the absolute permeability, *A* the cross-sectional area of porous medium, and Δp the differential pressure across the core. The f_i's at the outlet of the core are determined from the slopes of tangents drawn to the recovery curves. The term in brackets in Eq. 3 is evaluated from the graph of differential pressure vs PV injected, which is shown in Fig. 13. The differential pressure values at the intercepts of the tangents to this graph after breakthrough allow the calculation of this term.

4.6. Experimental Results

Three displacement experiments with different IFT pairs were conducted. All data are summarized in Table 8. After primary drainage of the C_{16}-rich phase by the NBA-rich phase up to the irreducible phase saturation, we found that the irreducible C_{16}-rich phase saturation was very high (61.5%) although we applied high injection flow rates. Since the porosity and absolute permeability of porous PTFE packs are very high, this high irreducible value of C_{16}-rich phase might have resulted from the plastic behavior of PTFE powder. After packing the PTFE powder, they take the ellipse-shaped form rather rounded solid beads. However it was not critical for our purposes.

Rapoport and Leas (1953) proposed a scaling coefficient for displacement experiments as,

$$lv_f\mu \quad (4)$$

where l is the length, v_f the front velocity, and μ the viscosity of displacing phase. For Experiments 1, 2, and 3 are $2.3\text{x}10^{-8}$ N, $3.4\text{x}10^{-8}$ N, and $5.6\text{x}10^{-8}$ N, respectively. These values are greater than the critical value of $0.835\text{x}10^{-9}$ N to $5.85\text{x}10^{-9}$ N, indicating that the displacement results should be independent of core length, flow rate, viscosity of injected fluid and capillary end effects.

In order to generalize the effect of capillary forces on trapping of oil within the pores of the reservoir rock during immiscible displacements, a dimensionless number, called the Capillary Number, has been used extensively in the literature. The capillary number is defined as the ratio of viscous to capillary forces:

$$N_{vc} = \frac{v\mu_D}{\sigma\cos\theta} \quad (5)$$

where v and μ_D are the velocity and viscosity, respectively, of the displacing fluid, and σ and θ are the IFT and contact angle, between the displacing and displaced fluids. The values of N_{vc} for the experiments are given in Table 8. As expected, the capillary effects between oil and gas phases decrease as IFT decreases, and hence the oil recovery is improved.

Figs. 14 and 15 show the recoveries of the C_{16}-rich and NBA-rich phases and the overall pressure drop across the core, respectively, recorded during each dynamic displacement of a mixture of C_{16}-rich and NBA-rich phases by H_2O-rich phase.

The recovery and pressure drop data after breakthrough were smoothed by fitting the data to an easily differentiable function before the analysis. By applying the Welge tangent construction method explained in Fig. 12 to the smoothed data we obtained a saturation path for the downstream end of the core. The saturation paths for each experiment are shown in Fig. 16. The solid dots marked on the edge of the ternary diagram represent the initial saturations in the reservoir before the gas (H_2O-rich phase) injection. During the dynamic displacement method we don't have any saturation or permeability data at the phase saturation values lower than the saturation at the front. This saturation shock (so-called Buckley-Leverett shock) causes the outflow saturation to jump to any lower part of the saturation trajectory. After breakthrough we have the drainage of the C_{16}-rich and NBA-rich phases and an increase in the H_2O-rich phase.

Using the JBN technique drawn in Fig. 13, we derived the relative permeabilities using the smoothed pressure data and Eq. 2 for each phase employed in the experiments. The fractional flows for each phase are determined from the slopes of the recovery curves.

4.7. Relative Permeabilities

Figs. 17-19 show the relative permeabilities to the C_{16}-rich, NBA-rich, and H_2O-rich phases, respectively.

Fig 17 shows a modest change in the relative permeability to the C_{16}-rich phase as IFT is varied. Many other works have shown that the wetting-phase relative permeability (k_{rw}) is a function of its own saturation and is independent of the initial saturation distribution. Sahni *et al.* (1998) found from their large experimental data that k_{rw} is a function of S_w^a, with a~5. Our data, however, correlates best to a third order polynomial, but have trends similar to those reported by Sahni *et al.* Also, in another work by Sahni *et al.* (1996), they obtained good agreement between fifth order polynomial and three-phase relative permeability data published by Grader and O'Meara (1988).

The relative permeability to the NBA-rich ("oil") phase shown in Fig. 18 is clearly dependent on the IFT variations. The data at high NBA-rich phase saturations fitted well by the correlation $k_{ro} \sim S_o^2$, which is represented by the dashed line on the figure. Many researchers have obtained this correlation for oil relative permeability and many of them also concluded that the oil relative permeability was a function of its own saturation only and independent of initial condition (Blunt, 2000). Our data actually deviate from the quadratic correlation at low saturations. We fitted the data best with a third order polynomial. At lower saturations the data converge to a constant oil saturation, presumably trapped oil in some pores. The existence of this so-called residual oil might be due to non-spreading conditions or to the nature of porous medium. It has been established that three-phase flow in a porous medium is clearly affected by spreading coefficient, which is defined by

$$C_s = IFT_{gw} - \left(IFT_{ow} + IFT_{go}\right) \qquad (6)$$

Within some experimental error, the spreading coefficients for Experiments 1, 2, and 3 are calculated from the IFT data as –0.071, 0.362, 0.011 mN/m, respectively. According to these values, in the first experiment, the oil is trapped between the gas and water phases whereas in other experiments, oil is supposed to flow between other two phases as layer drainage. However, in relatively rapid displacement experiments like ours, it is very difficult to see such layer drainage of oil. Slower gravity drainage experiments will be required to establish whether layer drainage does occur in these systems.

The gas relative permeabilities (Fig. 19) are also sensitive to IFT variations, as expected due to the fact that the composition and physical properties of the H_2O-rich phase ("gas") change with IFT variation. The experimental data for H_2O-rich phase relative permeabilities show trends similar trends to those observed for NBA-rich phase ("oil") relative permeabilities. The data obtained were fit with reasonable accuracy by a third order polynomial.

Additional experiments with lower IFTs around the critical tie line and with different initial conditions will be performed to investigate effects of near-critical flow in the presence of a third phase.

The experiments performed so far demonstrate that there is a significant effect of IFT on the flow of the nonwetting phases.

5. Conclusions

A four-component three-liquid-phase quaternary phase diagram has been determined that will allow investigation of the effects of IFT variation on three-phase flow. The phase diagrams demonstrate that three-phase systems can be created that exhibit low IFT between one pair of phases, a situation that is analogous to that created in multicontact miscible gas injection processes with water present. The IFT variation obtained for the three-phase hydrocarbon/alcohol/water system is consistent with that of gas/oil/water system under reservoir conditions.

Use of the analog liquids instead of real reservoir fluids requires the use of appropriate porous medium because of system wettability. Teflon bead packs have been employed in the displacement experiments to simulate the water-wet porous media with the analog liquids.

Three dynamic displacement experiments with IFTs of 0.028, 0.308, and 2.297 mN/m of NBA-rich phase ("oil") - H_2O-rich phase ("gas") pairs have been performed. The relevant three-phase relative permeabilities have been obtained from the recovery and pressure drop data by applying the JBN method. The wetting phase (C_{16}-rich) relative permeability is not affected by the IFT variation whereas the relative permeabilities to oil and gas phases are clearly affected. As IFT decreases the NBA-rich and H_2O-rich phases become more mobile at the same phase saturations.

6. References

Welge, H. J.: *A simplified method for computing oil recovery by gas or water drive*. AIME Trans. Vol. 195, p. 91, 1952.

Rapoport, L.A. and Leas, W.J.: *Properties of linear waterfloods*. AIME Trans. Vol. 198, p. 139, 1953.

Johnson, E.F., Bossler, D.P., and Naumann, V.O.: *Calculation of relative permeability from displacement experiments*. AIME Trans. Vol. 216, p. 370, 1959.

Manning, C.D. and Scriven, L.E.: *On interfacial tension measurement with a spinning drop in gyrostatic equilibrium*. Rev. Sci. Instrum., Vol. 48, No. 4, April 1997, 77.

Bardon, C. and Longeron, D.: *Influence of very low interfacial tensions on relative permeability*. SPE 7609, presented at the 53rd Annual Tech Conf and Exhib, Houston, TX, Oct 1-3 1978.

Morrow, N.R. and McCaffery, F.G.: *Fluid displacement studies in uniformly wetted porous media*. In Wetting, Spreading and Adhesion, Ed. J.F. Padday, Academic Press, N.Y., 1978, 289-319.

Knickerbocker, B.M., Peskeck, C.V., Davis, H.T., and L.E. Scriven: *Patterns of three-liquid-phase behavior illustrated by alcohol-hydrocarbon-water-salt mixtures*. J. Phys. Chem., 86, 393-400, 1982.

Delclaud, J., Rochon, J. and Nectoux, A.: *Investigation of gas/oil relative permeabilities: High-permeability oil reservoir application*. SPE 16999, presented at the 62rd Ann. Tech. Conf. and Exhib., Dallas, TX, 1987.

Grader, A.S. and O'Meara, D.J.: *Dynamic displacement measurements of three-phase relative permeabilities using three immiscible liquids*. SPE 18293, presented at the SPE 63rd Ann. Tech. Conf. and Exhib., Houston, TX, Oct. 2-5, 1988.

Asar, J. and Handy, L.L.: *Influence of interfacial tension on gas/oil relative permeability in a gas condensate system*. SPE Reservoir Eng., Feb. 1988, 257.

Morrow, N.R., Chatzis, I., and Taber, J.J.: *Entrapment and mobilization of residual oil in bead packs*. SPE 14423, SPE Reservoir Engineering, 927-935, August 1988.

Schechter, D.S., Zhou, D., and Orr, F.M., Jr.: *Low IFT drainage and imbibition*. J. of Pet. Sci. and Eng., 11, 283-300, 1994.

Sahni, A., Guzman, R. and Blunt, M.: *Theoretical analysis of three-phase flow experiments in porous media*. SPE 36664, presented at the SPE Ann. Tech. Conf. and Exhib., Denver, CO, Oct. 6-9, 1996.

Kontogeorgis, G.M., Voutsas, E.C., Yakournis, I.V., and Tassios, D.P.: *An equation of state for associating fluids*. I&EC Res., 35, 1996, 4310.

Buckley, J., Liu, Y., Xie, X., and Morrow, N.: *Asphaltenes and crude oil wetting – The effect of oil composition*. SPE 35366, SPE Journal, Vol. 2, June, 1997.

Raal, J.D. and A.L. Muehlbauer: *Phase equilibria – Measurement and computation*. Taylor & Francis Publishers, Washington DC, 1997, 461 p.

Tehrani, D.H., Henderson, G.D., Danesh, A., Al-Siyabi, Z., and Salino, P.A.: *Effect of interfacial tension on gas and oil relative permeability (Part I-Primary drainage)*. Paper P554 presented at the 59th EAGE Conf. And Tech. Exhib., Geneva, 1997.

McDougall, S.R., Salino, P.A., and Sorbie, K. S.: *The effect of interfacial tension upon gas-oil relative permeability measurements: Interpretation using pore-scale models*. SPE 38920, presented at the 1997 SPE Annual Technical Conf. and Exhib., San Antonio, TX, 5-8 Oct.

Sahni, A., Burger, J.H. and Blunt, M.: *Measurement of three phase relative permeability during gravity drainage using CT scanning*. SPE 39655, presented at the SPE/DOE IOR Symposium, Tulsa, Oklahoma, Apr. 19-22, 1998.

Blunt, M.: *An empirical model for three-phase relative permeability*. SPE Journal, 5 (4), p. 435, December, 2000.

Mulyadi, H. and Amin, R.: *A new approach to 3D reservoir simulation: Effect of interfacial tension on improving oil recovery*. SPE 68733, presented at the SPE Asia Pacific Oil and Gas Conf. and Exhib., Jakarta, Indonesia, Apr. 17-19, 2001.

Table 1 – Some research related to the effect of low IFT on performance of gas-oil displacements.

	Porous Medium	Fluids used and IFT range	Remarks
Bardon & Longeron (1978)	Fontaineblaue sandstone ϕ = 0.099 k = 83 mD	C_1-nC_7 0.001 - 12.5 mN/m	k_r invariant for IFT>0.04 mN/m k_r tends to be straight lines for IFT<0.04 mN/m
Asar & Handy (1983)	Berea sandstone ϕ = 0.2 k = 193 mD	C_1-C_3 0.03 – 0.82	k_r invariant for IFT>0.18 mN/m k_r tend to be straight lines for IFT<0.18 mN/m
Delclaud *et al* (1987)	Different samples ϕ = 0.07 to .246 k=33-1480 mD	Air- oil 0.6 – 30	k_r are unchanged with IFT
Tehrani *et al* (1997)	Reservoir core samples ϕ = 0.087 k=44.2 mD	C_1-nC_{10} 0.019 – 9.76	k_{rg} is more sensitive to IFT changes than k_{ro} Less variations in the oil permeability

Table 2 – Compositional data for Fig.3.

Sample		**Components**							
		Mass fraction				**Mole fraction**			
		NBA	**C_{16}**	**IPA**	**H_2O**	**NBA**	**C_{16}**	**IPA**	**H_2O**
Mix 1	C_{16}-rich	0.119	0.876	0.000	0.005	0.2783	0.6736	0.0000	0.0481
	NBA-rich	0.739	0.167	0.000	0.094	0.6259	0.0465	0.0000	0.3276
	H_2O-rich	0.082	0.000	0.000	0.918	0.0212	0.0000	0.0000	0.9788
	Overall	0.284	0.312	0.000	0.404	0.1386	0.0501	0.0000	0.8113
Mix 2	C_{16}-rich	0.083	0.880	0.025	0.012	0.1834	0.6393	0.0681	0.1091
	NBA-rich	0.654	0.107	0.103	0.136	0.4754	0.0256	0.0923	0.4067
	H_2O-rich	0.077	0.000	0.053	0.870	0.0207	0.0000	0.0176	0.9617
	Overall	0.271	0.298	0.045	0.385	0.1349	0.0488	0.0276	0.7887
Mix 3	C_{16}-rich	0.057	0.905	0.027	0.011	0.1316	0.6870	0.0769	0.1045
	NBA-rich	0.563	0.061	0.182	0.194	0.3506	0.0125	0.1398	0.4971
	H_2O-rich	0.095	0.000	0.087	0.818	0.0266	0.0000	0.0301	0.9433
	Overall	0.258	0.284	0.091	0.366	0.1310	0.0474	0.0570	0.7646
Mix 8	C_{16}-rich	0.062	0.898	0.026	0.014	0.1387	0.6606	0.0718	0.1289
	NBA-rich	0.493	0.035	0.214	0.258	0.2694	0.0063	0.1442	0.5801
	H_2O-rich	0.118	0.000	0.106	0.776	0.0343	0.0000	0.0380	0.9277
	Overall	0.193	0.271	0.110	0.426	0.0889	0.0410	0.0625	0.8075
Mix 8b	C_{16}-rich	0.058	0.898	0.027	0.017	0.1271	0.6468	0.0730	0.1532
	NBA-rich	0.415	0.022	0.227	0.336	0.1991	0.0035	0.1343	0.6632
	H_2O-rich	0.146	0.000	0.129	0.725	0.0444	0.0000	0.0484	0.9072
	Overall	0.169	0.239	0.138	0.454	0.0739	0.0344	0.0745	0.8172
Mix 9	C_{16}-rich	0.053	0.903	0.027	0.017	0.1170	0.6552	0.0735	0.1544
	NBA-rich	0.305	0.009	0.211	0.475	0.1209	0.0012	0.1032	0.7748
	H_2O-rich	0.207	0.000	0.168	0.625	0.0693	0.0000	0.0694	0.8613
	Overall	0.179	0.263	0.151	0.407	0.0842	0.0407	0.0876	0.7876

Table 3 – Compositional data for Fig. 4.

Sample		Components					
		Mass fractions			Mole fractions		
		NBA	IPA	H_2O	NBA	IPA	H_2O
Mix 12T	NBA-rich	0.826	0.000	0.174	0.5357	0.0000	0.4643
	H_2O-rich	0.082	0.000	0.918	0.0212	0.0000	0.9788
	Overall	0.500	0.000	0.500	0.1955	0.0000	0.8045
Mix 5T	NBA-rich	0.635	0.130	0.235	0.3603	0.0910	0.5487
	H_2O-rich	0.105	0.053	0.842	0.0289	0.0180	0.9531
	Overall	0.490	0.109	0.401	0.2154	0.0591	0.7254
Mix 7T	NBA-rich	0.517	0.182	0.301	0.2611	0.1134	0.6255
	H_2O-rich	0.118	0.089	0.793	0.0338	0.0314	0.9347
	Overall	0.348	0.143	0.509	0.1329	0.0674	0.7998
Mix 6T1	NBA-rich	0.383	0.203	0.414	0.1639	0.1071	0.7290
	H_2O-rich	0.130	0.124	0.746	0.0388	0.0456	0.9156
	Overall	0.326	0.185	0.489	0.1270	0.0889	0.7840
Mix T12	NBA-rich	0.315	0.205	0.480	0.1239	0.0994	0.7767
	H_2O-rich	0.137	0.136	0.727	0.0416	0.0509	0.9075
	Overall	0.235	0.174	0.591	0.0816	0.0745	0.8440

Table 4 – Compositional data for Fig. 5.

Sample		Components					
		Mass fractions			Mole fractions		
		C_{16}	IPA	H_2O	C_{16}	IPA	H_2O
Mix 1T	C_{16}-rich	1.000	0.000	0.000	1.0000	0.0000	0.0000
	H_2O-rich	0.001	0.000	0.999	0.0001	0.0000	0.9999
	Overall	0.500	0.000	0.500	0.0740	0.0000	0.9260
Mix T15	C_{16}-rich	0.967	0.030	0.003	0.8641	0.0993	0.0366
	H_2O-rich	0.002	0.320	0.679	0.0002	0.1238	0.8760
	Overall	0.400	0.200	0.400	0.0650	0.1219	0.8131
Mix 2T	C_{16}-rich	0.950	0.046	0.004	0.8128	0.1491	0.0381
	H_2O-rich	0.003	0.565	0.432	0.0004	0.2814	0.7182
	Overall	0.300	0.402	0.298	0.0542	0.2723	0.6735
Mix T8	C_{16}-rich	0.933	0.063	0.004	0.7681	0.1948	0.0371
	H_2O-rich	0.050	0.810	0.140	0.0102	0.6270	0.3628
	Overall	0.300	0.599	0.101	0.0787	0.5896	0.3317
Mix T14	C_{16}-rich	0.916	0.082	0.002	0.7335	0.2475	0.0190
	H_2O-rich	0.062	0.817	0.122	0.0133	0.6592	0.3275
	Overall	0.370	0.551	0.079	0.1080	0.6034	0.2886
Mix T16	C_{16}-rich	0.894	0.105	0.001	0.6873	0.3032	0.0095
	H_2O-rich	0.083	0.824	0.093	0.0191	0.7127	0.2681
	Overall	0.380	0.561	0.059	0.1179	0.6530	0.2291
Mix T18	C_{16}-rich	0.850	0.147	0.003	0.5907	0.3832	0.0261
	H_2O-rich	0.115	0.815	0.070	0.0284	0.7552	0.2164
	Overall	0.484	0.480	0.036	0.1770	0.6583	0.1647
Mix T23	C_{16}-rich	0.770	0.226	0.004	0.4617	0.5083	0.0300
	H_2O-rich	0.237	0.730	0.033	0.0699	0.8082	0.1219
	Overall	0.481	0.499	0.020	0.1848	0.7191	0.0961

Table 5 – Density, viscosity, and IFT data.

Samples		**Mix 1**	**Mix 2**	**Mix 3**	**Mix 8**	**Mix 8b**	**Mix 9**
Density (g/cm^3)	C_{16}-rich	0.776	0.774	0.774	0.772	0.772	0.773
	NBA-rich	0.824	0.837	0.846	0.858	0.870	0.903
	H_2O-rich	0.987	0.983	0.976	0.969	0.960	0.946
Viscosity (mPa.s)	C_{16}-rich	2.942	3.071	3.065	3.046	3.084	3.111
	NBA-rich	2.973	3.145	3.279	3.237	3.510	3.749
	H_2O-rich	1.216	1.563	1.824	1.833	2.416	3.043
IFT (mN/m)	C_{16}-rich / H_2O-rich	2.465	2.068	1.893	1.776	1.749	1.622
	C_{16}-rich / NBA-rich	0.239	0.551	0.794	1.106	1.491	1.583
	NBA-rich / H_2O-rich	2.297	1.157	0.654	0.308	0.086	0.028

Table 6 – Correspondence of analog and reservoir phases.

Analog Liquids	Water-wet reservoir system (Oil-wet lab system) (Teflon beads packing)	Oil-wet reservoir system (Water-wet lab system) (Glass beads packing)
C_{16}-rich phase	WATER	WATER
NBA-rich phase	OIL	GAS
H_2O-rich phase	GAS	OIL

Table 7 – Contact angles of analog liquids in the Teflon and glass tubing.

Composition from base tie triangle	Phase in which contact angle measured	Contact angle, degrees	
		Glass capillary (ID 0.2mm)	Teflon tubing (ID 0.2mm)
C_{16}-rich / NBA-rich	C_{16}-rich	143 (NBA-rich wets)	38 (C_{16}-rich wets)
C_{16}-rich / H_2O-rich	C_{16}-rich	108 (H_2O-rich wets)	45 (C_{16}-rich wets)
NBA-rich / H_2O-rich	H_2O-rich	76 (H_2O-rich wets)	138 (NBA-rich wets)

Table 8 – Data for the displacement experiments

Exp #	Fluid (Tab 2)	IFT mN/m	Initial Condition		q mL/min	Capillary Number $x10^{-5}$		Total Recovery
		NBA-rich / H_2O-rich	S_{oi}	S_{wi}		C_{16}-rich / H_2O-rich	NBA-rich / H_2O-rich	PVI≈1.5
1	Mix 1	2.297	0.208	0.792	1.51	3.58	3.65	0.508
2	Mix 8	0.308	0.190	0.810	1.52	7.24	41.4	0.609
3	Mix 9	0.028	0.191	0.809	1.50	13.9	745.2	0.632

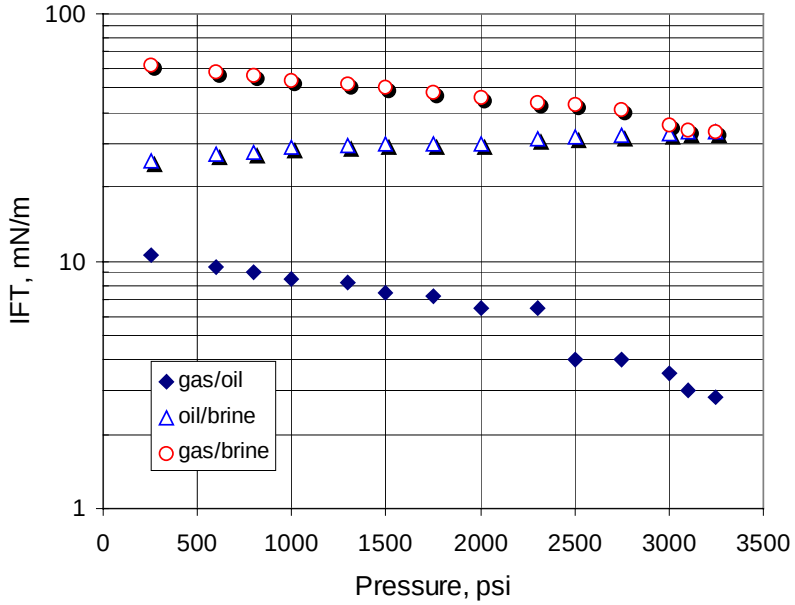

Figure 1 – IFT between oil, gas and brine phases as a function of pressure at reservoir conditions [Mulyadi and Amin, 2001].

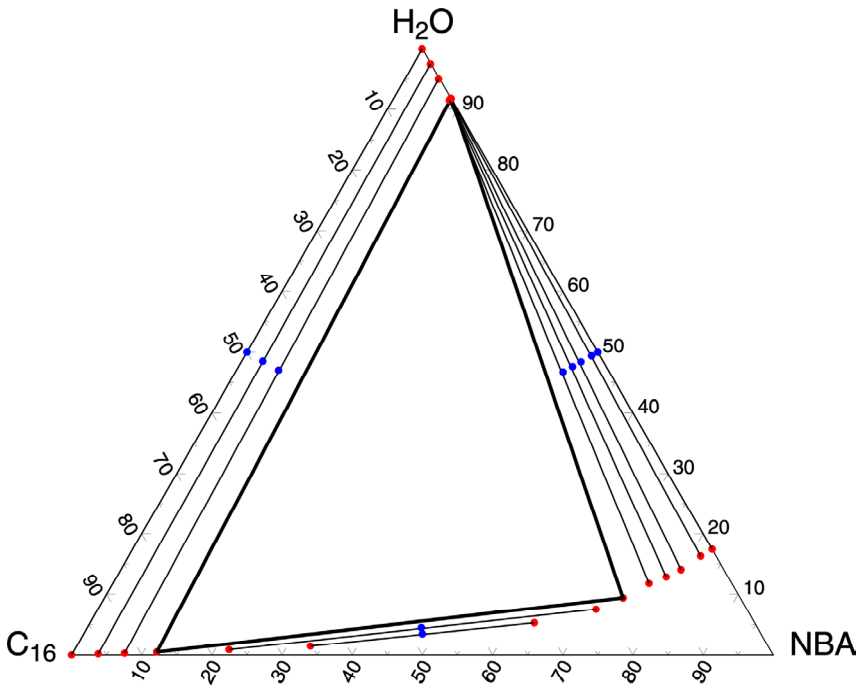

Figure 2 – Ternary phase diagram for the C_{16}/NBA/H_2O system.

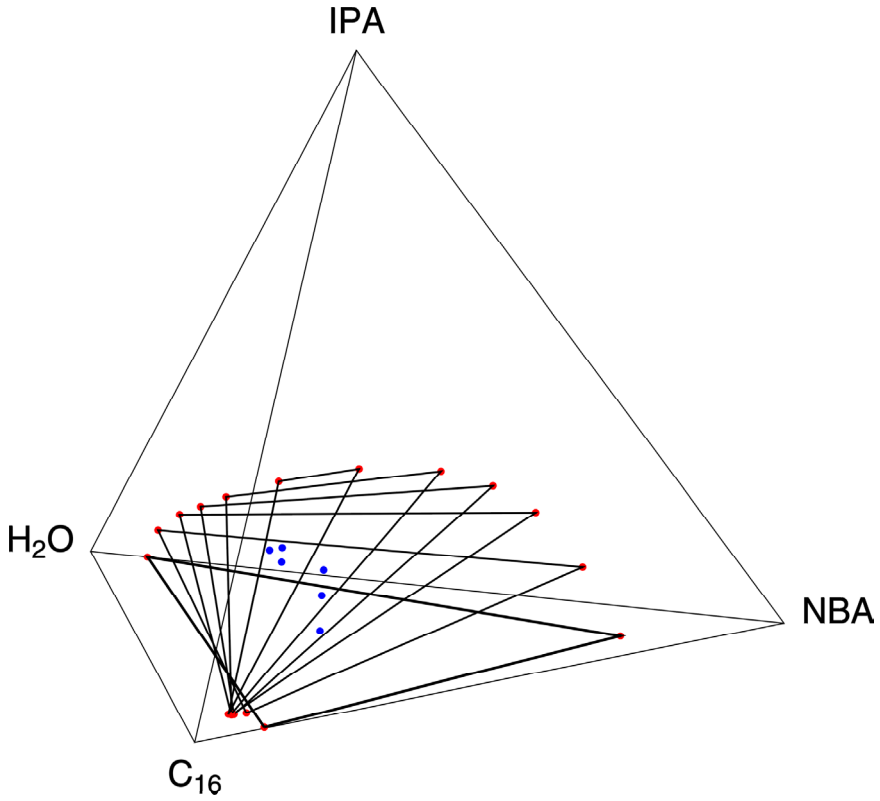

Figure 3 – Sequence of tie triangles representing the three-phase region.

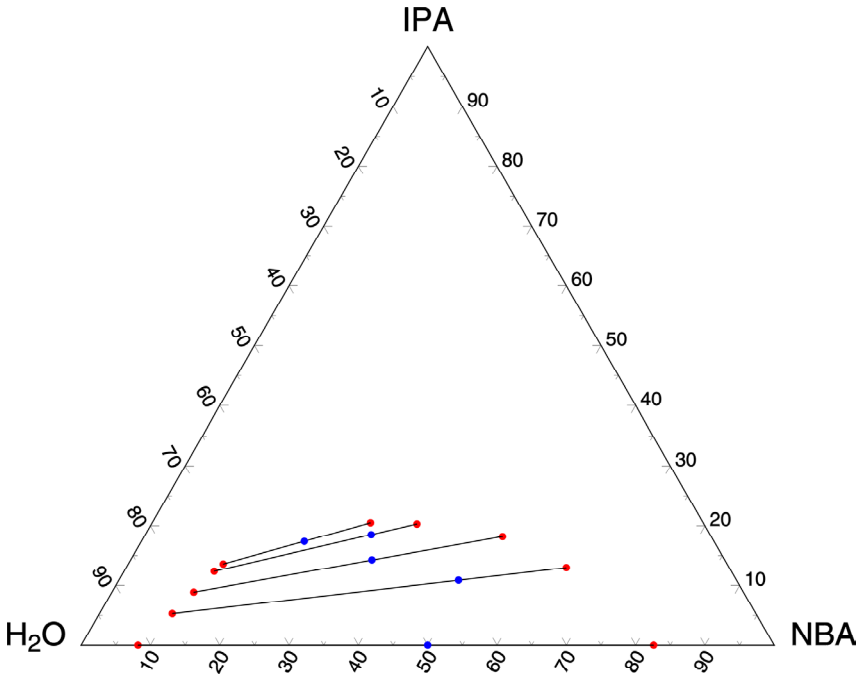

Figure 4 – Tie lines for the NBA/IPA/H_2O system.

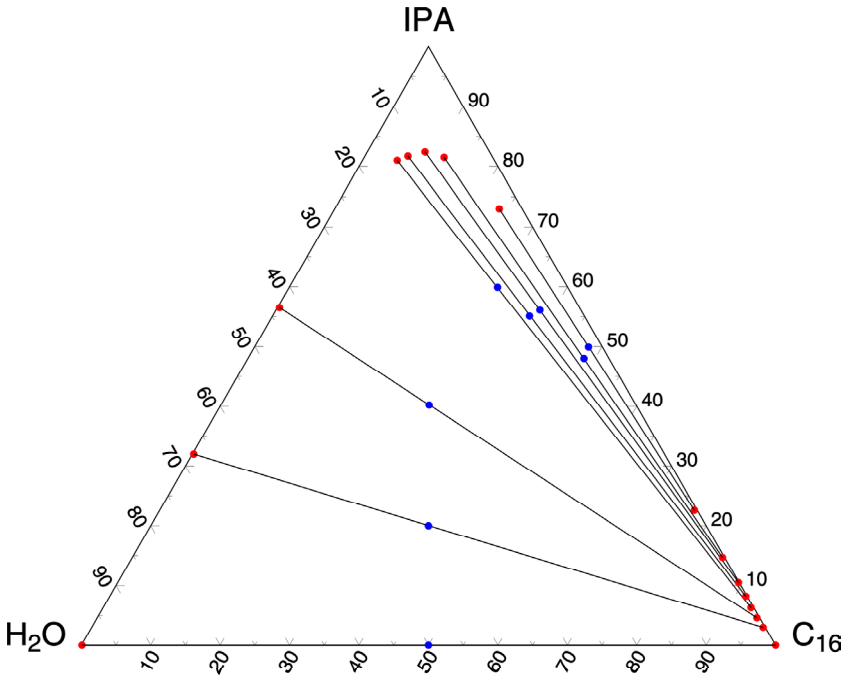

Figure 5 – Tie lines for the C_{16}/IPA/H_2O system.

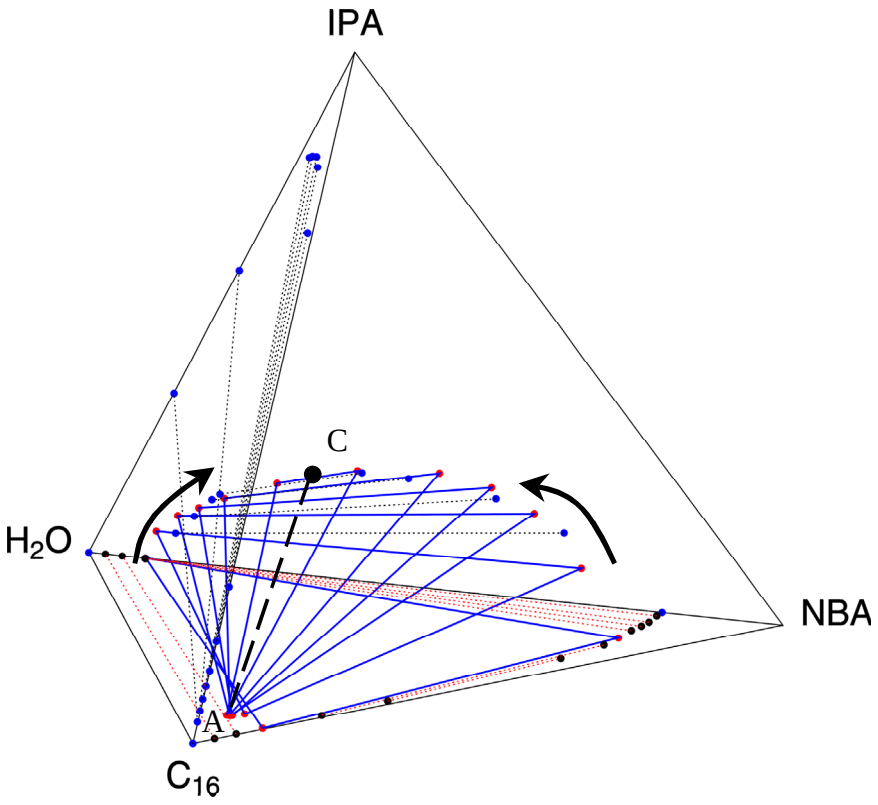

Figure 6 – Quaternary phase diagram for the C_{16}/NBA/H_2O/IPA system.

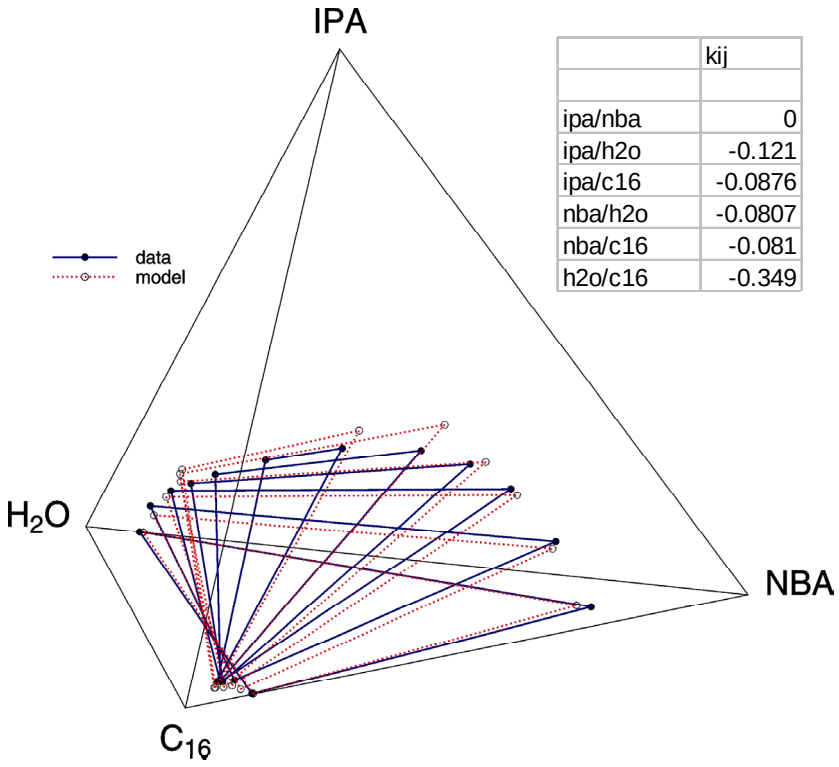

	kij
ipa/nba	0
ipa/h2o	-0.121
ipa/c16	-0.0876
nba/h2o	-0.0807
nba/c16	-0.081
h2o/c16	-0.349

Figure 7– Soave-Redlich-Kwong+Association (CPA) model for 3-phase compositional data.

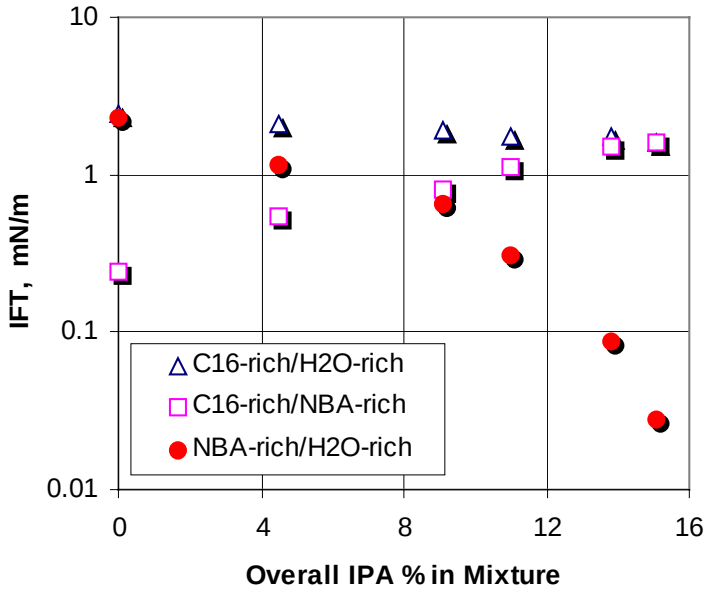

Figure 8 – IFT variation of C_{16}/NBA/H_2O/IPA system as a function of overall IPA fraction in the mixture.

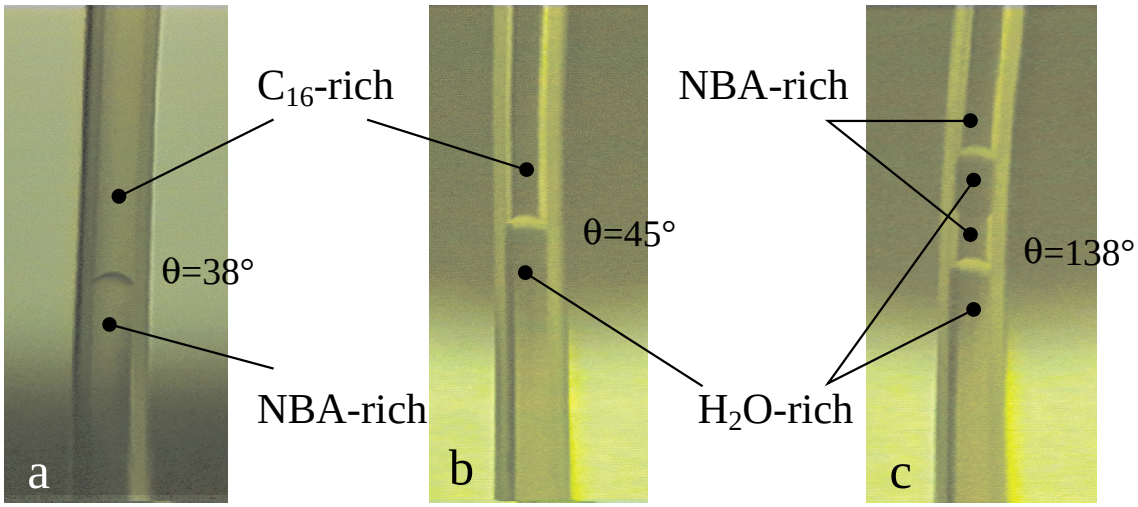

Figure 9 – Coexistence of analog liquids in the PTFE tubing.

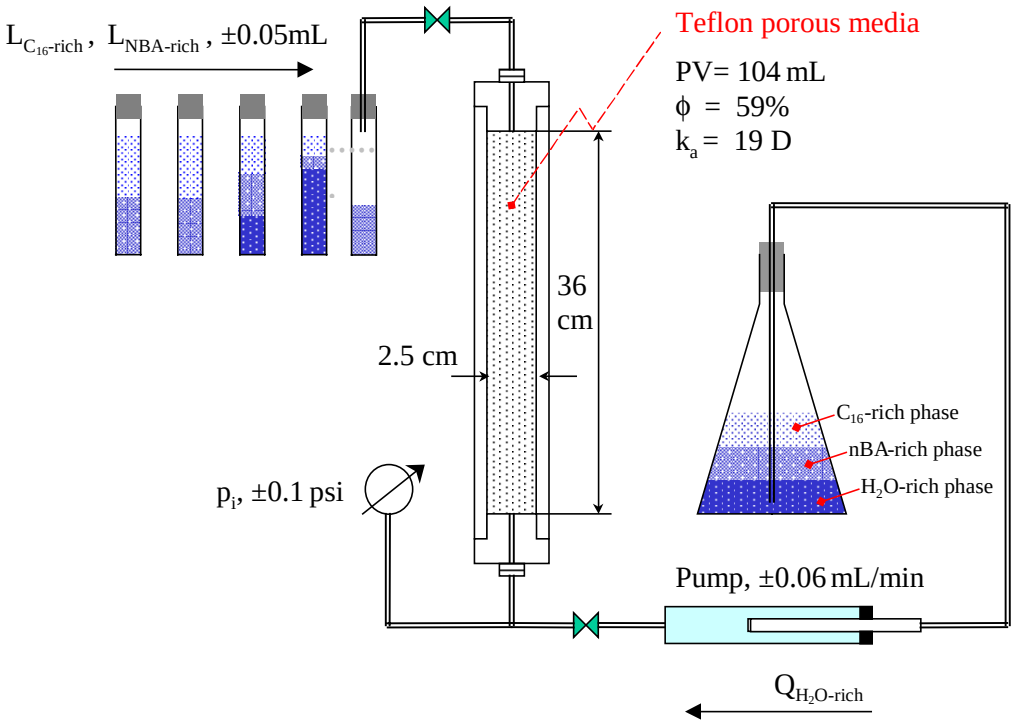

Figure 10 – Experimental equipment for displacement experiments.

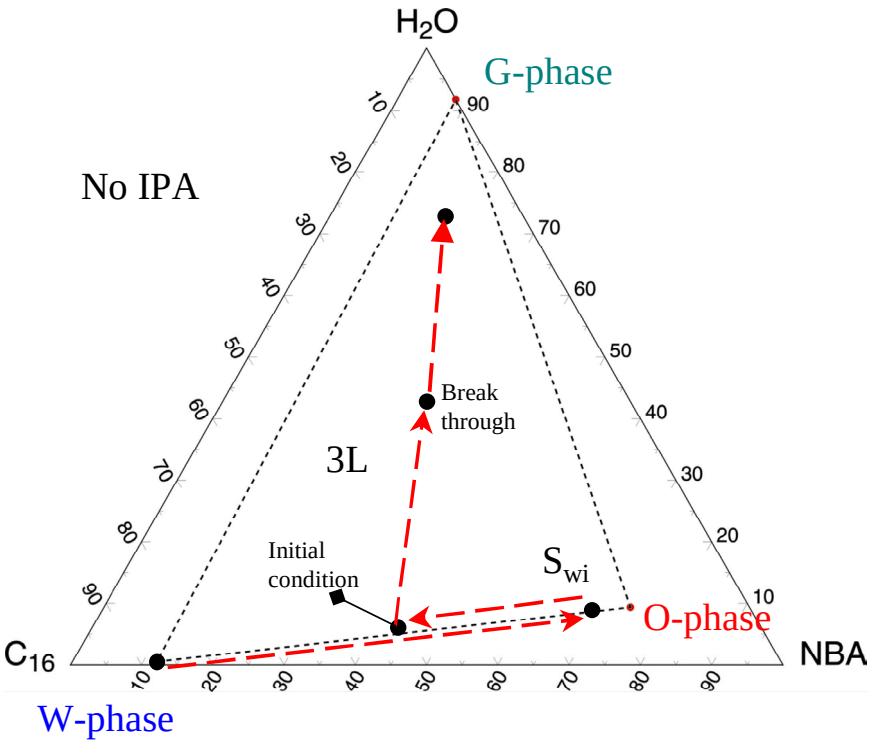

Figure 11 - A sample saturation path for three-phase flow.

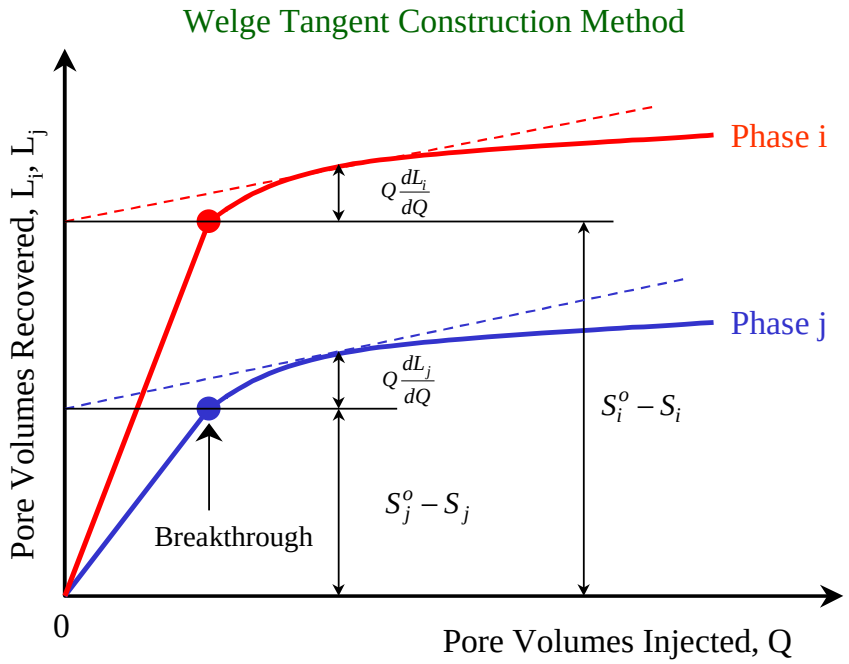

Figure 12 – The Welge method for the determination of saturations at the end of the core.

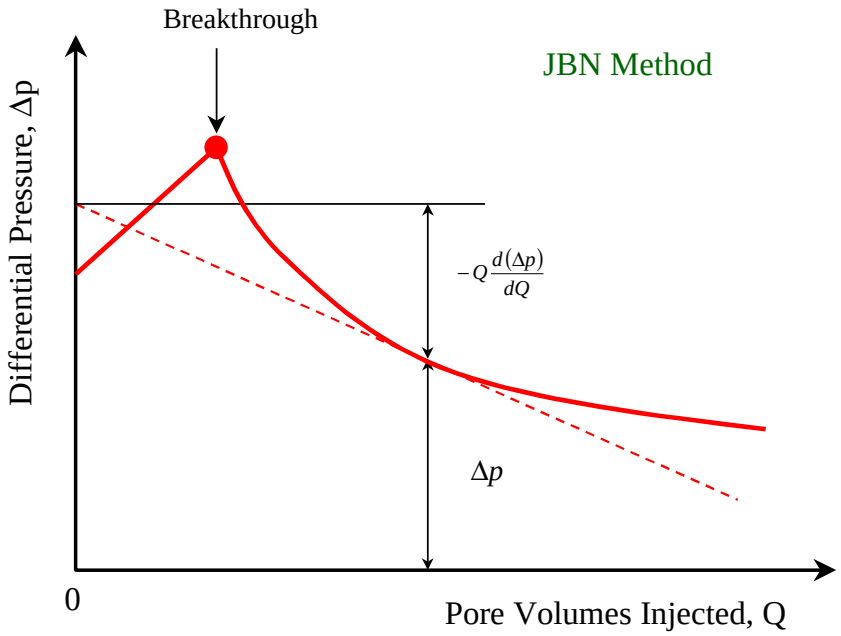

Figure 13 – The JBN method for the determination of the pressure gradient at the end of the core.

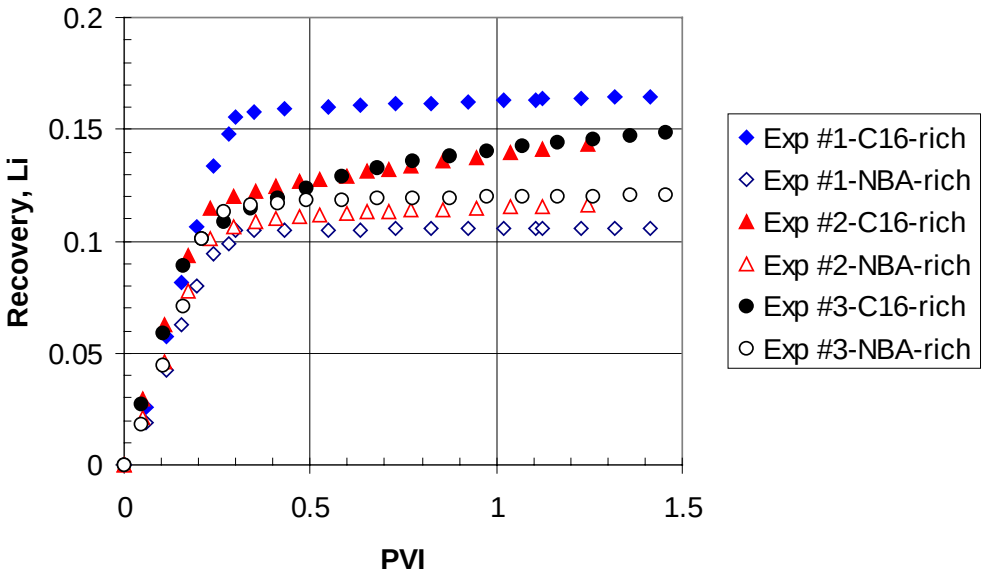

Figure 14 – Pore volume effluents as a function of pore volumes injected.

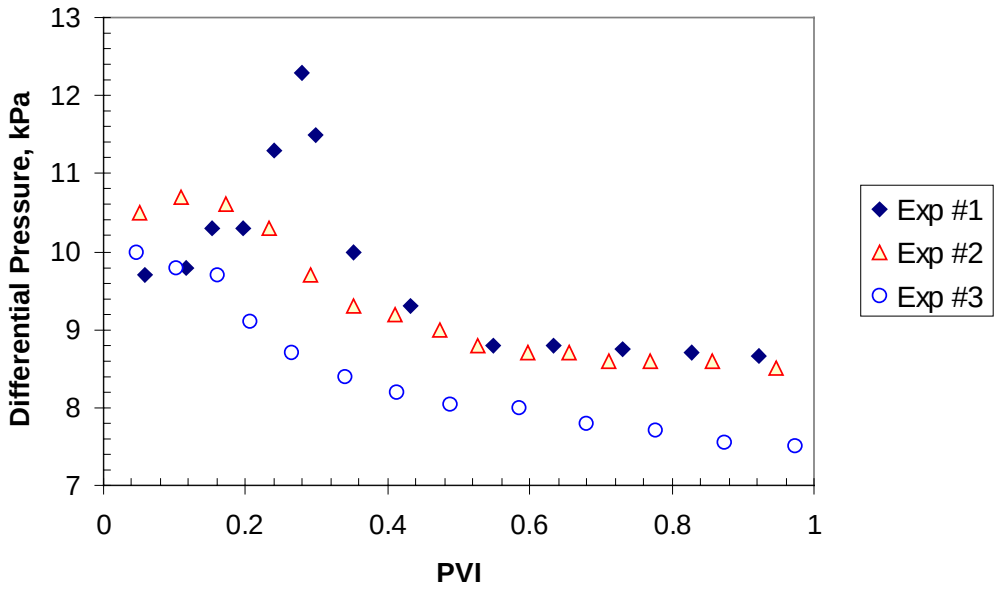

Figure 15 – Pressure drop as a function of pore volumes injected.

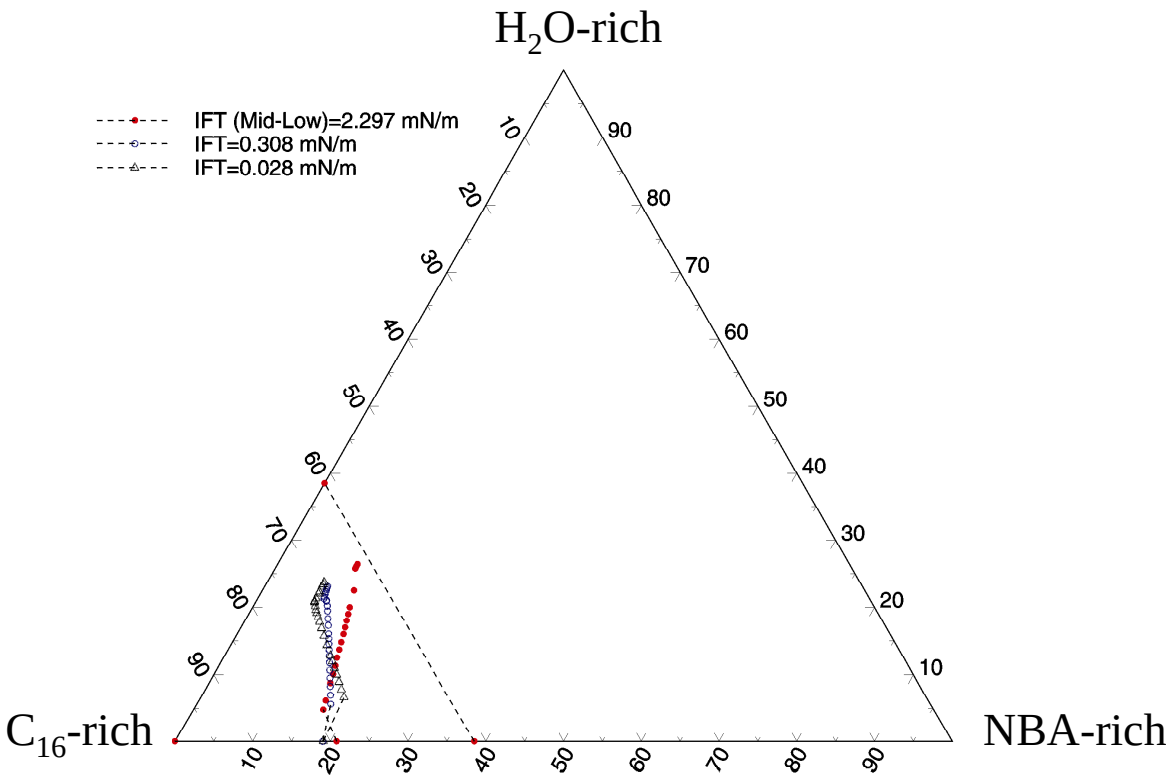

Figure 16 – Saturation paths for the displacement experiments.

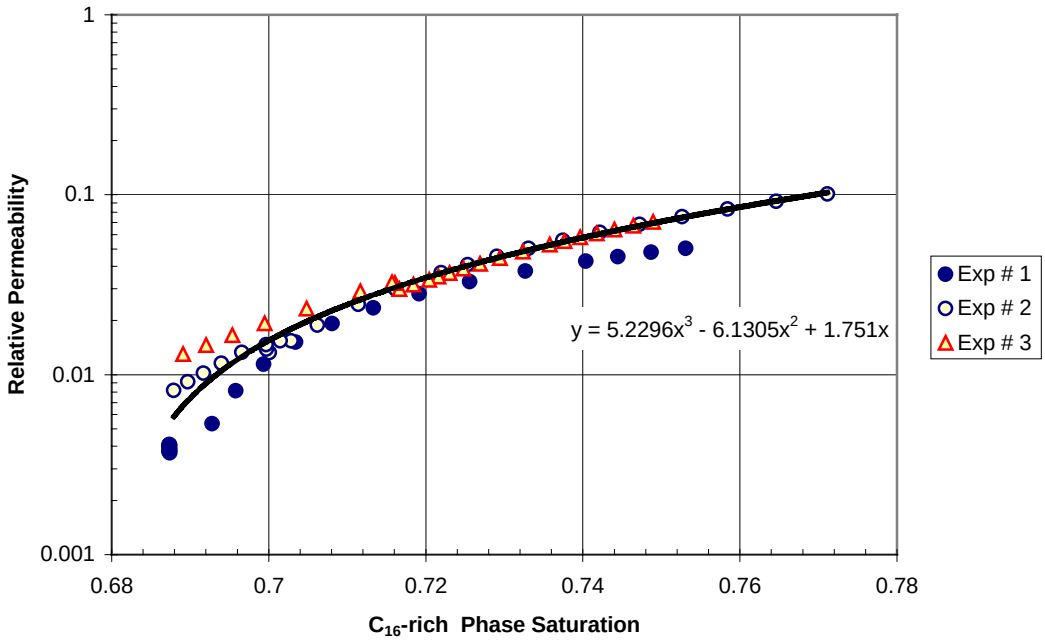

Figure 17 – Relative permeability of C_{16}-rich (WATER) phase as a function of own saturation.

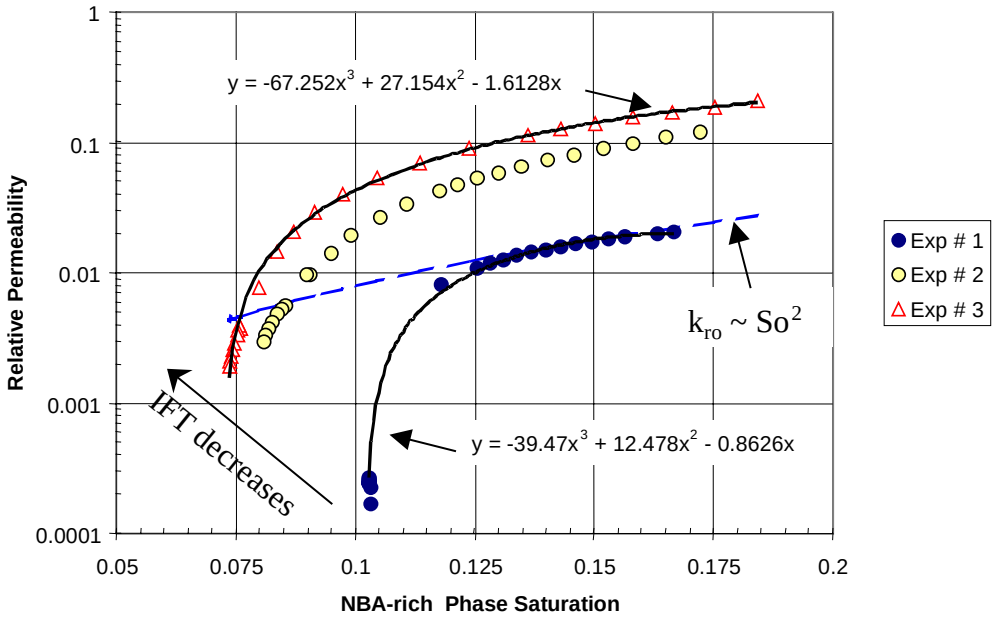

Figure 18 – Relative permeability of NBA-rich (OIL) phase as a function of own saturation.

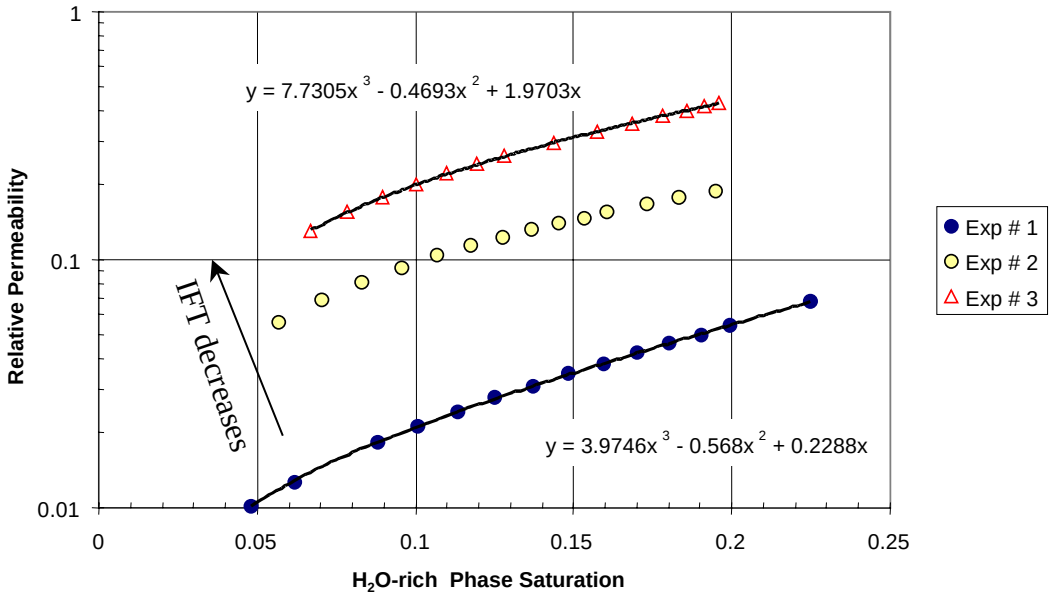

Figure 19 – Relative permeability of H_2O-rich (GAS) phase as a function of own saturation.